Research Article

^{19}F chemical shifts, coupling constants and conformational preferences in monosubstituted perfluoroparacyclophanes

Ion Ghiviriga,[a]* Lianhao Zhang,[a] Henry Martinez,[a] Rubén H. Contreras,[b] Cláudio F. Tormena,[c] Laura Nodin[a] and William R. Dolbier Jr[a]

In the process of studying the chemistry of perfluoro[2.2]paracyclophanes (PFPCs), a novel class of compounds, it became necessary to identify some disubstituted products. To achieve this goal, we characterize in this work some monosubstituted PFPCs, identifying their ^{19}F–^{19}F coupling patterns, and establishing a methodology for the assignment of their ^{19}F chemical shifts. The pattern of coupling constants indicates a skewed geometry in which the upper deck moves towards or away from the substituent, depending on the substituent electron-donor character and size. Quantum chemical calculations, performed at the HF/6-311 + G(d,p)//B3LYP/EPR-III level of theory, confirmed the conformations inferred from coupling constants and reproduced well the values of the couplings. Transmission mechanisms for the FC term of four- and five-bond ^{19}F–^{19}F couplings are discussed in detail. Understanding the conformational preferences of PFPCs and how they are reflected by the coupling constants facilitates the assignment of ^{19}F chemical shifts in monosubstituted PFPCs and the identification of the disubstituted products. Copyright © 2011 John Wiley & Sons, Ltd.

Supporting information may be found in the online version of this article.

Keywords: NMR; ^{19}F–^{19}F couplings; ^{19}F chemical shifts; perfluoro[2.2]paracyclophane; paracyclophane; conformation; FCCP-CMO; Fermi hole; through-space

Introduction

The aromatic rings of perfluoro[2.2]paracyclophane (PFPC) are extremely reactive with respect to nucleophilic substitution reactions.[1] With oxygen-based nucleophiles, such as hydroxide, alkoxide and aryloxide, monosubstituted products were generally formed, in most cases along with di- and multisubstituted products, depending on the conditions of the reaction and the number of equivalents of nucleophile used. On the other hand, for nucleophiles such as aryl thiolates, which upon substitution serve to activate the substituted ring towards further substitution, only multisubstituted products were obtained. For example, in the reaction of PFPC with phenyl thiolate, one disubstituted product was produced, as well as two *tetra*-substituted and one *hexa*-substituted product. The oxygen-based nucleophiles generally produced more than one disubstituted product. There are seven possible disubstituted isomers, which are the *ortho, meta* and *para* isomers, bearing both substituents on the same benzene ring, and the *pseudo-ortho, pseudo-meta, pseudo-para* and *pseudo-geminal*, which have the substituents on different rings. Thus, it has become essential that we develop methodology that will allow us to distinguish the various multisubstituted PFPCs.

As the first step towards being able to do this, we present herein a methodology for the assignment of the ^{19}F chemical shifts in *monosubstituted* PFPCs, based on ^{19}F–^{19}F coupling constants, reporting all such assignments for compounds 1–8 (Fig. 1). Few ^{19}F–^{19}F coupling constants and virtually no assignments of such couplings for substituted PFPCs have been reported thus far.[1]

Transmission mechanisms of the Fermi contact (FC) term corresponding to $^4J(F_9S,F_5)$, $^4J(F_{10}S,F_{12})$, $^5J(F_{10}S,F_5)$ and $^5J(F_9S,F_{12})$

^{19}F–^{19}F coupling constants are rationalized, taking 4 as a model compound (Fig. 1). These data will be used in future work for the elucidation of the regiochemistry of multisubstituted PFPCs.

Experimental

All of the NMR spectra, except for the ^{19}F–^{1}H HOESY, were recorded on a three-channel Varian Inova spectrometer, equipped with a 5-mm indirect detection probe, ^{1}H–^{19}F/^{13}C/X, operating at 500 MHz for ^{1}H, and 470 MHz for ^{19}F. The solvent was benzene-d_6, and the temperature 25 °C. ^{1}H chemical shifts were referenced to the solvent, 7.14 ppm for ^{1}H on the tetramethylsilane scale. ^{19}F chemical shifts were referenced to Ξ = 94.0940478 corresponding to 0 ppm for CFCl$_3$.
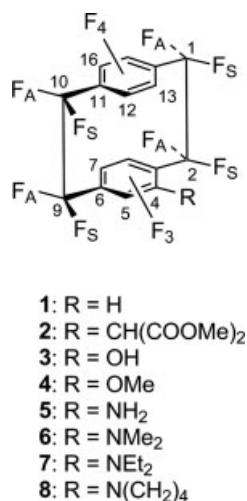
^{19}F spectra were recorded with a spectral window from -92 to -152 ppm (28 200 Hz) in 16 transients, with an acquisition time of 2 s and a relaxation delay of 0 s, with a 90° pulse width. The FID was zero-filled to 131 072 points and weighed with a line broadening function prior to the Fourier transform.

* Correspondence to: Ion Ghiviriga, Chemistry Department, University of Florida, Gainesville, FL 32611-7200, USA. E-mail: ion@chem.ufl.edu

a Chemistry Department, University of Florida, Gainesville, FL 32611-7200, USA

b Departamento de Física, FCEyN, U. B. A. and IFIBA-CONICET, Cdad. Universitaria, Pab. I, 1428 Buenos Aires, Argentina

c Organic Chemistry Department, Chemistry Institute, University of Campinas, 13084-971 Campinas, São Paulo, Brazil

1: R = H
2: R = CH(COOMe)₂
3: R = OH
4: R = OMe
5: R = NH₂
6: R = NMe₂
7: R = NEt₂
8: R = N(CH₂)₄

Figure 1. Monosubstituted PFPCs in this study and position numbering. The geminal bridge fluorines are labeled *S* or *A*, being *syn* or *anti* to the substituent, correspondingly.

The $^{19}F-^{19}F$ DQF-COSY spectra were recorded on the minimum spectral window which included all of the signals. The number of points for the spectrum was 8192 in both dimensions. The same number of points was acquired in *f*2, in eight transients per increment, with a relaxation delay of 1 s. The number of increments was 4096. The FIDs were weighted with a line broadening function prior to the Fourier transform.

$^{19}F-^{1}H$ HOESY spectrum of 7 was taken on a Varian Mercury spectrometer, operating at 300 MHz for ^{1}H and 282 MHz for ^{19}F. The probe was a 5-mm conventional probe, with the high-band coil simultaneously tuned to ^{1}H and ^{19}F. The 90° pulses were 9.1 and 13.5 µs, correspondingly. The solvent was toluene-d_8 and the temperature −60 °C. Phase-sensitive HOESY spectra were acquired with observation on ^{19}F, in 8192 points, on a spectral window from -92 to −142 ppm (14 100 Hz). The relaxation delay was 0.8 s, and the number of scans per increment was 1024. A number of 256 increments were used in *f*1, on a spectral window of 1000 Hz. Zero-filling twice to 1024 points was used in *f*1, which afforded a resolution slightly larger than 1 Hz/point. The mixing time was 0.01 s, the optimum value found in an array of mixing times of 0.002, 0.005, 0.01, 0.02, 0.05 and 0.1 s for *pseudo-ortho*-difluoro-AF4.[2]

The rates for rotation (*k*) have been measured in toluene-d_8 by line-shape analysis using gNMR,[3] in the temperature range −50 to 20 °C for the diethylamino compound 7, and −65 to −45 °C for the dimethylamino compound 6. The temperature was raised on automation in steps of 5 °C, and 20 min were allowed for temperature equilibration before shimming at each temperature. The reading of the thermocouple was corrected according to the methanol standard. The activation parameters $\Delta H^{\#}$ and $\Delta S^{\#}$ for rotation have been calculated from the slope and intercept of the line $\ln(k/T)$ *versus* 1/*T*. The points fit the line with an $R^2 > 0.992$.

Spin–spin coupling calculations reported in this work were performed at the HF/6-311+G(d,p)//B3LYP/EPR-III level of theory using the Gaussian 03[4] package of programs. Canonical molecular orbitals (CMOs) expanded in terms of natural bond orbitals were obtained using the NBO 5.0 program.[5]

The syntheses of all compounds discussed in this paper, other than compounds 1 and 5, have been previously reported.[1]

4-Hydroperfluoro[2.2]paracyclophane, 1

To a solution of PFPC (250 mg, 0.504 mmol, 1 eq.) in THF, 12 ml was added at −30 °C LiAlH(O^{t}Bu)$_3$ (0.756 ml of a 1.0-M solution in THF, 0.756 mmol, 1.5 eq.) during 30 min. The reaction mixture was stirred at −30 °C for 4 h. The residue was purified by column chromatography (silica gel, hexanes) to give a mixture of 4-hydroperfluoro[2.2]paracyclophane (i) and dihydroperfluoro[2.2]paracyclophane (a 1 : 1 mixture of *pseudo-meta* and *pseudo-para*) (ii), in a 6 : 4 ratio (87% yield combined). (i) HR-MS *m/z* calcd for C₁₆HF₁₅ 477.9839 [M⁺], found 477.9822. (ii) HR-MS *m/z* calcd for C₁₆H₂F₁₄ 459.9933 [M⁺], found 459.9925.

**4-Aminoperfluoro[2.2]paracyclophane, 5**

To a solution of ammonium hydroxide (28.8%, 200.5 mg, 1.65 mmol) in anhydrous THF (10 ml) was added PFPC (372 mg, 0.75 mmol). The reaction mixture was stirred at RT overnight and then concentrated to dryness. The residue was purified by column chromatography (silica gel, hexanes/dichloromethane = 9 : 1) to give 4-aminoperfluoro[2.2]paracyclophane (5) (330 mg, 89.3%) as a yellow solid: mp 214–215 °C; ^{1}H NMR, δ 4.60 (br. s, 2H); anal. calcd for C₁₆H₂F₁₅N: C 38.97, H 0.41, N 2.84; found: C 39.18, H 0.29, N 2.73.

Results and Discussion

Methodology for the assignment of the ^{19}F chemical shifts

Monosubstituted PFPCs 1–8 display a multitude of $^{19}F-^{19}F$ couplings, ranging from *ca.* 250 Hz for the geminal coupling to couplings smaller than 3 Hz, which are visible only when the line is not broaden by other small couplings. Couplings over 3 Hz were identified in the DQF-COSY spectrum, were confirmed and measured in selective decoupling experiments, and were refined through simulation in gNMR.[3] The experimental and simulated spectra for compound 2 are given in Fig. 2. Chemical shifts and coupling constants are collected in Table 1.

Only the largest couplings were used for the assignment of the fluorine signals. We have previously demonstrated that in mono- and di-fluoro-1,1,2,2,9,9,10,10-octafluoro[2.2] paracyclophane (fluoro-AF4s), a bridge fluorine couples with a large coupling constant (20–30 Hz) with the aromatic fluorine *ortho* and *syn*, and with a somehow smaller constant (20–10 Hz) with the aromatic fluorine which is *pseudo-gem* to the fluorine *ortho* and *syn*.[2] The other large couplings used for the assignment were the *ortho* coupling of the aromatic fluorines, 28–18 Hz, significantly larger than the *meta* or *para* couplings, 12–0 Hz.[6] The steps of the assignment procedure on the example of compound 2 are presented in Fig. 3: (a) the pairs of geminal fluorines were identified by a large coupling, *ca.* 250 Hz. (b) Couplings larger than 50 Hz identified the aromatic fluorines (a9, a14, a15) *ortho* and *syn* to some of the bridge fluorines (a8, a7 and a6, correspondingly). (c) Couplings of 10–40 Hz of these latter bridge fluorines identified the aromatic fluorines (a13, a10 and a11) *pseudo-gem* to their *ortho* and *syn* partners. (d) Other couplings larger than 10 Hz of these latter aromatic fluorines (a13, a10 and a11) identified the bridge protons *ortho* and *syn* to them (a3, a2 and a4, correspondingly), which established the identity and relative orientation of the fluorines in a tetrafluoroethane unit. In most cases, this assignment can be confirmed by couplings of 8–10 Hz between the bridge fluorines which are vicinal and *syn*. The aromatic fluorines that are *pseudo-gem* display
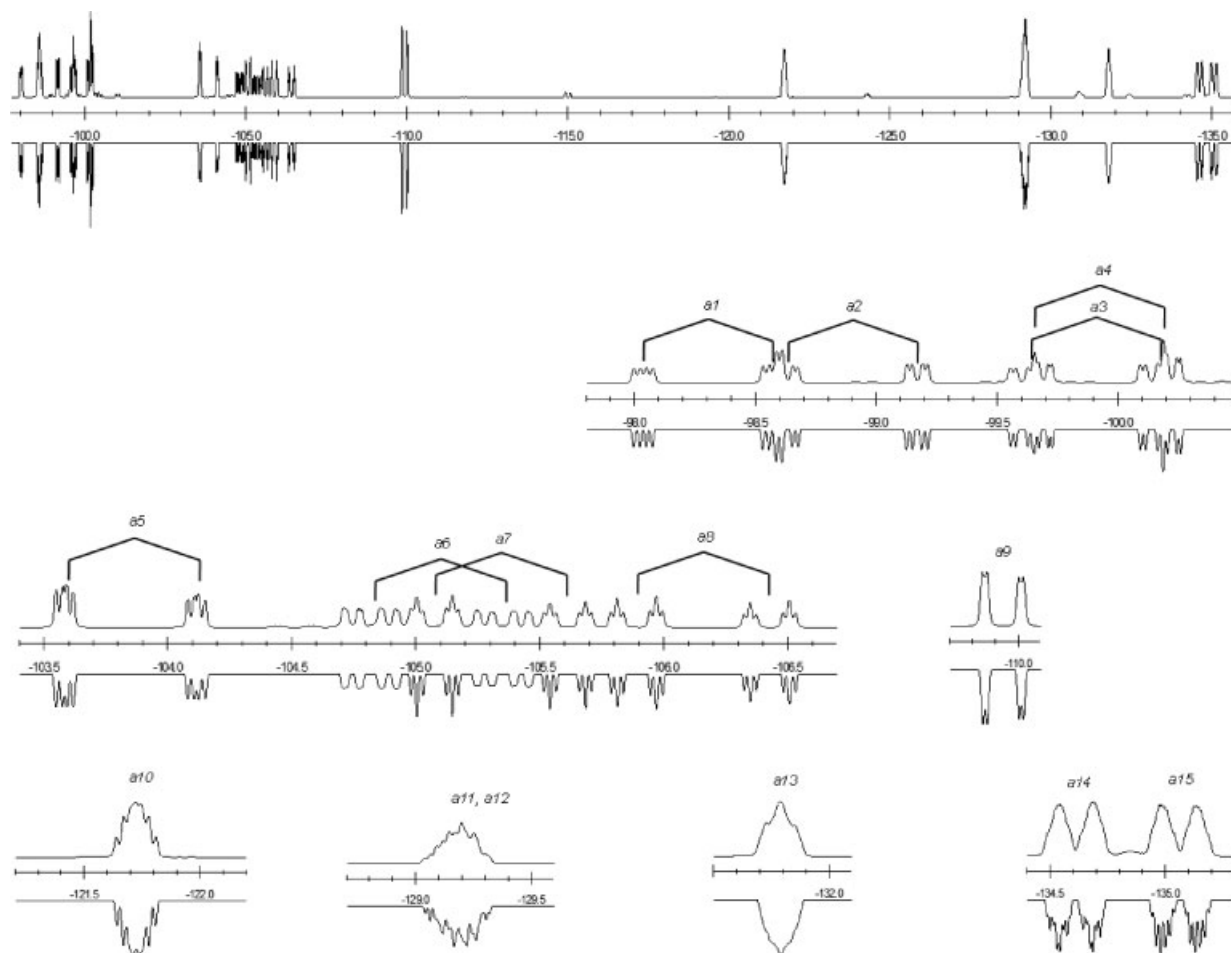
Figure 2. ^{19}F spectrum of compound 2, experimental (top) and simulated (bottom).

Table 1. Chemical shifts (ppm) and coupling constants (Hz) in the ^{19}F spectrum of compound 2

	δ	J_{an-a1}	J_{an-a2}	J_{an-a3}	J_{an-a4}	J_{an-a5}	J_{an-a6}	J_{an-a7}	J_{an-a8}	J_{an-a9}	J_{an-a10}	J_{an-a11}	J_{an-a12}	J_{an-a13}	J_{an-a14}
$a1$	−98.31														
$a2$	−98.91														
$a3$	−99.88														
$a4$	−99.98														
$a5$	−103.83	12.0			249.8										
$a6$	−105.07	250.7			8.0										
$a7$	−105.33		12.0	252.2											
$a8$	−106.15		252.0	10.0											
$a9$	−109.93		2.0	2.0						74.2					
$a10$	−121.72		29.8			3.5	11.5								
$a11$	−129.14				25.6		28.1				9.0	22.0			
$a12$	−129.24	24.3				21.0									
$a13$	−131.79			33.2			4.0		13.0	3.0			20.0		
$a14$	−134.61							67.4			14.7		6.0	6.0	
$a15$	−135.06	2.0				69.7						10.0	8.0	8.0	20.0

a coupling of *ca.* 10 Hz, similar to that observed in *pseudo-gem* difluoroparacyclophane.[7] The couplings with aromatic fluorines of the bridge fluorines in the tetrafluoroethane unit *a*2, *a*3, *a*7, *a*8 display a 'diagonal pattern', i.e. the bridge fluorines displaying couplings over 50 Hz with the *ortho* and *syn* and couplings over

10 Hz with the fluorines *pseudo-gem* to the ones *ortho* and *syn*, are vicinal and *anti*. This diagonal pattern can be applied to assign *a*12 as *ortho* and *syn* to *a*1, since *a*12 displays couplings with comparable constants with both *a*1 and *a*5. The position of *a*12 can also be established later on, based on the *ortho* coupling of the aromatic

fluorines. (e) Just one *ortho* coupling of the aromatic fluorines is necessary at this point to join the two 'half-molecules' determined in step (d). The other two *ortho* couplings confirm the whole assignments and determine/confirm the position of the aromatic fluorines which display comparable couplings with two bridge ones, like *a*12. There are cases, however, where the *ortho* couplings are difficult to identify, due to the numerous couplings of the aromatic fluorines. The coupling constants for couplings between aromatic fluorines have been measured as the loss in the width of the line at half-height when the coupling partner is selectively irradiated and are less accurate than the ones involving aliphatic fluorines. In an alternative approach, the cross-peaks in the DQF-COSY spectrum of the fluorine *pseudo-gem* to the substituent identify the fluorines of the 'upper deck', narrowing the possibilities for joining the two halves of molecule from four to two. Of these two possibilities, we chose the one that satisfies the diagonal relationship, i.e. the aromatic fluorines having the largest $^4J_{syn}$ are *ortho*.

The complete assignments of the signals of 2 are given on the structure in Fig. 3(f). Alternately, the positions of the fluorines in the representation of Fig. 3(e) are given in Fig. 3(g).

The assignment of the ^{19}F chemical shifts in compounds 1–8 is given in Tables 2–9.

### Coupling constants, chemical shifts and preferred conformations

The ^{19}F spectrum of 2 (Fig. 1) displays a pattern for the bridge fluorines which was seen in all of the compounds 2–8, namely there are four more shielded and four more deshielded fluorines, and each of the fluorines in the deshielded region has a geminal partner in the shielded region. Three or four of the most shielded bridge fluorines display the largest coupling constants with the aromatic fluorine over four bonds and *syn*. Rae *et al.* have demonstrated that $^4J_{syn}$ is at a maximum when the dihedral angle is 0.[8] The bridge fluorines with the largest $^4J_{syn}$ are on one side of the 'upper deck' of the PFCP (e.g. F_1A and $F_{10}A$ in 2) and on the opposite side of the 'lower deck' (F_9S in 2), suggesting a skewed geometry in which the upper deck moves towards or away from the substituent. In a move towards the substituent, F_1S, F_2A, F_9A and $F_{10}S$ are drawn closer to both the aromatic fluorine four bonds away and *syn* and to the aromatic fluorine on the remote deck five bonds away and *syn*. The case described above corresponds to compounds 3–5. In compounds 1, 2 and 6–8, F_9S, $F_{10}A$ and F_1A display larger $^4J_{syn}$ couplings both over four bounds with the aromatic *syn* fluorines in agreement with a move of the upper deck away from the substituent. This would be expected for 2 and 6–8 if the size of the substituent were the factor defining the 'away' form. However, compound 1, which has the smallest substituent, adopts the 'away' geometry, found for larger substituents. This suggests that a different interaction should define such geometry. Since in the current literature[9] examples are discussed where it is concluded that two stacked fluorinated aromatic planes undergo attractive interactions, it could be expected that in perfluoroparacyclophanes a similar attraction would take place. This interaction should be affected by the presence of a substituent attached to one of the benzene rings. Of course, bulky substituents like in compound 2 would counteract such stacking interaction. Similar effect would be expected if an F atom is replaced by an H atom since the stacking interaction would be decreased in the neighborhood of the latter; this would be the case of compound 1. Besides, it is also known[10,11] that a lone-pair bearing atom can be attracted by similar π aromatic system. For this reason, it
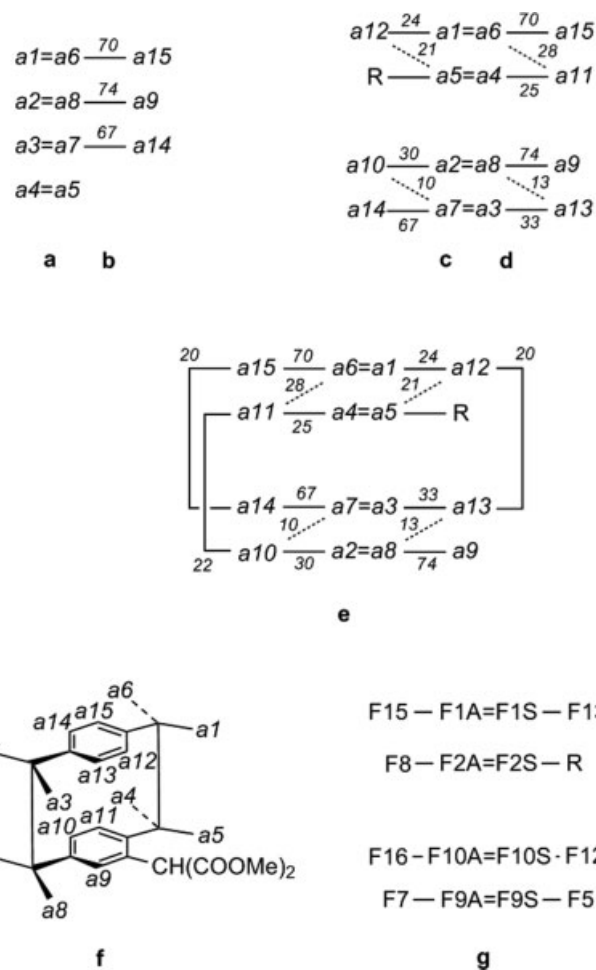
Figure 3. a–e Step-by-step assignment of the 19F signals in compound 2: a) geminal bridge fluorines are identified by a 250 Hz coupling; b) Couplings larger than 50 Hz identify the aromatic fluorines *ortho* and *syn* to some of the bridge fluorines; c) other couplings larger than 10 Hz of these bridge fluorines identify the aromatic fluorines pseudo-gem to their ortho and syn partners; d) couplings larger than 10 Hz of these later aromatic protons identified the bridge fluorines ortho and syn to them; e) one ortho coupling, ca. 20 Hz of the aromatic fluorines joins the two half-molecules determined in step d. f) assignment of the signals in compound 2. g) position numbering in the representation of Fig. 3(e).

would not be surprising if in compounds 3–5 where an F atom is replaced by a substituent containing a lone-pair bearing atom in the α position the towards conformation is preferred. In all three cases, such lone pairs conjugate strongly with the π electronic system of the lower deck. In fact, according to this description, it is expected that in 3–5 there is an attractive interaction between the substituent and the upper deck, favoring a 'towards'' geometry.

Geometry optimizations performed at the HF/6-311+G(d,p) level of theory confirmed the conformations inferred from coupling constants (Fig. 4). The more stable conformation (Fig. 4) for compound 1, which has the upper deck away from hydrogen atom is 0.6 kcal/mol lower in energy than the conformation having the upper deck towards the hydrogen atom. An opposite behavior was observed for compound 4, where the conformation having the upper deck towards the methoxy group was 2.14 kcal/mol lower in energy than the conformation having the upper deck away from the substituent. The diethylamino compound 7 preferred the 'away' conformation by 5.00 kcal/mol. The optimized geometry for
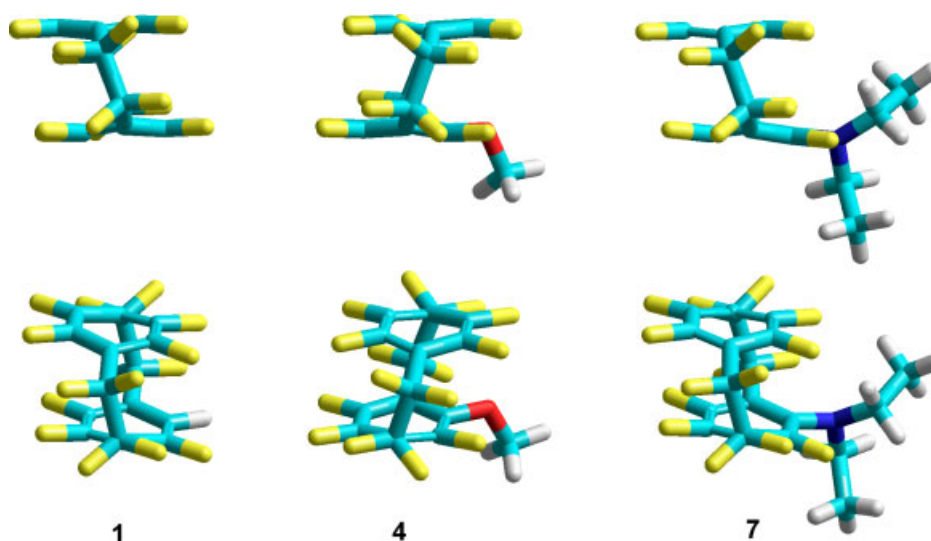
Figure 4. Calculated most stable conformations for compounds 1, 4 and 7.

compound 4 shows also an interesting effect on vicinal couplings between bridge fluorine atoms. It is found that the F_1S-F_2S distance, $d(F_1S-F_2S) = 2.431$ Å, whereas $d(F_1A-F_2A) = 2.412$ Å, i.e. the 'towards' movement lengthens the former and shortens the latter. They must be compared with the calculated $d(F_{10}A-F_9A) = 2.420$ Å and $d(F_{10}S-F_9S) = 2.421$ Å, in the same compound 4. All these distances are notably shorter than twice the F van der Waals radius, i.e. $2 \times 1.47 = 2.94$ Å and it suggests that the respective FC term of $syn\ ^3J_{FF}$ couplings are quite sensitive to such a distance. According to values reported in Table 5, $^3J(F_1S-F_2S) = 5$ Hz, while $^3J(F_1A-F_2A) = 12$ Hz, supporting nicely the assumption about the overlap between the respective fluorine electron clouds being one important coupling pathway for these vicinal J_{FF} couplings. However, it is interesting to note that this distortion of the bridge is not indicative of the 'towards' or 'away' conformation of the upper deck since similar effects are observed for such experimental vicinal couplings in compound 8. This trend is easy to rationalize considering that these vicinal couplings show very important SD, FC and PSO contributions and their dependence on geometry are quite different from those of the FC term.

Other small (2–5 Hz) $^{19}F-^{19}F$ long-range couplings between aromatic and bridge fluorines in 1–8 have been noticed in the DQF-COSY spectra and have then been optimized through simulation in gNMR. They display an angular dependence which parallels the one of the $^1H-^1H$ couplings. The bridge fluorine which is further away from the plane of the aromatic ring displays a small (ca. 5 Hz) coupling with the aromatic fluorine four bonds away and anti. This is similar to the cisoid allylic coupling, which reaches a maximum when the C–H bond of the allyl proton is perpendicular to the plane of the double bond.[12] The bridge fluorine which is closer to the plane of the aromatic ring and displays a coupling over 50 Hz with the aromatic fluorine ortho and syn also displays a coupling over five bonds with the aromatic fluorine meta and anti. Similar couplings between the benzylic proton in the plane of the aromatic ring and the proton meta and anti have been reported.[13]

The trends in the chemical shifts, $^4J_{syn}$ and $^5J_{syn}$, are presented in Fig. 5. $^4J_{syn}$ in Fig. 5(c) display very good clustering for the two geometries. A line at 50 Hz separates the values for the 'towards' and 'away' conformations. The values of $^4J_{syn}$ for positions 9 and 10 in compounds 2–8 depend, apparently, on the size of the

substituent, and so do the values of $^5J_{syn}$ for positions 1A and 2S, when not null. For instance, the values of $^4J_{syn}$ in positions 9A and 10S in 1 are larger than in the same positions of 2 and 6–8, whereas the values in positions 1S, 1A and 2A are comparable. This suggests an equilibrium between the away conformer and a twisted one, in which the C_9-C_{10} bridge is towards and the C_1-C_2 bridge is away. The chemical shifts in positions 1A, 9S, 9A, 10S and 10A (Fig. 5(a)) depend mainly on the conformation, as do, to a lesser extent, the chemical shifts of the aromatic fluorines of the 'upper deck'. $^4J_{syn}$ are similar to those described by Mallory et al.[14] and depend strongly on the F–F distance between the coupling nuclei. It is highlighted that this assumption is further supported as follows. There is a fluorine deshielding effect of 6.35 ppm reported by Mallory et al.[14] when going from 1-F-4,5-dimethylnaphthalene to 1,8-difluoro-4,5-dimethylnaphthalene; the latter is a compound whose $^4J_{syn}$ follows the 'normal' trend with the F–F distance. On the other hand, for compounds that follow the 'abnormal' trend, the proximity between both fluorine atoms renders a shielding effect, e.g. compounds 4b and 4c from Mallory et al.'s paper. It is observed in Tables 2–9 that the F_9S shielding correlates approximately with the respective $^4J_{syn}$ coupling, i.e. the proximity of both fluorine atoms yields a shielding effect on F_9S. It should be recalled that the 'abnormal' behavior reported by Mallory et al.[14] was afterwards[15] rationalized as originating in a substantial paramagnetic spin orbit (PSO), contributing to $^4J_{syn}$, which increases, in absolute value, when increasing the strain in the C–F bonds. Calculated coupling constants reported in Tables 10 and 11 are compatible with these comments and the F_9S shielding effect when increasing $^4J_{syn}$ suggests a rather strong bridge strain. As expected, the chemical shifts of F_1S, F_2A and F_2S, and of the aromatic protons on the 'lower deck' depend mainly on the substituent. The abnormal deshielding of positions 2S and 2A in compound 1 suggests a hydrogen bond between H4 and F_2S. In the preferential 'away' geometry, the existence of such hydrogen bond is further confirmed by the optimized F_2S-H distance, i.e. 2.35 Å, which is notably shorter than the sum of their van der Waals radii (1.20 + 1.47 = 2.67 Å). The chemical shifts of F_5, F_7 and F_8 in compounds 1–8 are similar to those in substituted pentafluorobenzenes.[6]

The calculated geometry of compound 7 displays a tilted diethylamino group, with a dihedral angle $C_5-C_4-N-C\alpha$ of −44°.

Table 2. NMR data for the (a) aliphatic fluorines and (b) aromatic fluorines in compound 1 in benzene-d_6

(a)

Position	δ (ppm)	^2J (Hz)	^3J (Hz)	$^4J_{syn}$ (Hz)	$^5J_{syn}$ (Hz)	Other ^nJ (Hz)
1S	− 101.61	255	7 (F$_1$A−F$_2$A)	28	–	<3 (F$_{15}$)
1A	− 105.85			71	15	<3 (F$_{12}$)
2S	− 109.29	242		–	18	<3 (F$_7$)
2A	− 108.06			22	0	
9S	− 104.62	253	9 (F$_9$A−F$_{10}$A); 9 (F$_9$S−F$_{10}$S)	61	12	<3 (F$_8$)
9A	− 101.24			44	0	<3 (F$_5$)
10S	− 101.15	253		46	0	<3 (F$_{16}$)
10A	− 104.59			62	12	

(b)

Position	δ (ppm)	$^3J_{ortho}$ (Hz)	$^4J_{meta}$ (Hz)	$^5J_{para}$ (Hz)	$^7J_{pseudo-gem}$ (Hz)
5	− 108.67	–	0	8	10
7	− 124.27	20	0	–	10
8	− 133.37		–	8	10
12	− 131.46	20	<3	8	10
13	− 128.71		<3	8	–
15	− 134.86	20	<3	8	10
16	− 134.25		<3	8	10

Table 4. NMR data for the (a) aliphatic fluorines and (b) aromatic fluorines in compound 3 in benzene-d_6

(a)

Position	δ (ppm)	^2J (Hz)	^3J (Hz)	$^4J_{syn}$ (Hz)	$^5J_{syn}$ (Hz)	Other ^nJ (Hz)
1S	− 102.27	249	11 (F$_1$A−F$_2$A)	63	–	3 (F$_{16}$)
1A	− 99.06			28	0	3 (F$_{13}$)
2S	− 98.92	244		–	0	3 (F$_8$)
2A	− 103.56			77	19	3 (F$_5$)
9S	− 100.14	249	11 (F$_9$A−F$_{10}$A); 8 (F$_9$S−F$_{10}$S)	30	0	3 (F$_7$)
9A	− 104.79			69	14	
10S	− 105.04	252		67	17	3 (F$_{15}$)
10A	− 100.29			31	0	3 (F$_{12}$)

(b)

Position	δ (ppm)	$^3J_{ortho}$ (Hz)	$^4J_{meta}$ (Hz)	$^5J_{para}$ (Hz)	$^7J_{pseudo-gem}$ (Hz)
5	− 131.90	–	6	9	15
7	− 148.56	20	6	–	10
8	− 138.67		–	9	10
12	− 136.48	20	8	5	15
13	− 134.91		6	8	–
15	− 132.12	20	6	5	10
16	− 133.96		8	8	10

Table 3. NMR data for the (a) aliphatic fluorines and (b) aromatic fluorines in compound 2 in benzene-d_6

(a)

Position	δ (ppm)	^2J (Hz)	^3J (Hz)	$^4J_{syn}$ (Hz)	$^5J_{syn}$ (Hz)	Other ^nJ (Hz)
1S	− 98.31	251	12 (F$_1$S−F$_2$S); 8 (F$_1$A−F$_2$A)	24	–	<3 (F$_{15}$)
1A	− 105.07			67	28	<3 (F$_{12}$)
2S	− 103.83	250		–	21	<3 (F$_7$)
2A	− 99.98			26	0	
9S	− 106.15	252	12 (F$_9$A−F$_{10}$A); 10 (F$_9$S−F$_{10}$S)	74	13	<3 (F$_8$)
9A	− 98.91			30	0	<3 (F$_5$)
10S	− 99.88	252		33	<3	<3 (F$_{16}$)
10A	− 105.33			67	12	<3 (F$_{13}$)

(b)

Position	δ (ppm)	$^3J_{ortho}$ (Hz)	$^4J_{meta}$ (Hz)	$^5J_{para}$ (Hz)	$^7J_{pseudo-gem}$ (Hz)
5	− 109.93	–	0	9	3
7	− 121.72	22	0	–	14
8	− 129.16		–	9	10
12	− 131.79	20	<3	8	10
13	− 129.19		<3	8	–
15	− 135.06	20	<3	8	10
16	− 134.61		<3	8	14

Table 5. NMR data for the (a) aliphatic fluorines and (b) aromatic fluorines in compound 4 in benzene-d_6

(a)

Position	δ (ppm)	^2J (Hz)	^3J (Hz)	$^4J_{syn}$ (Hz)	$^5J_{syn}$ (Hz)	Other ^nJ (Hz)
1S	− 104.39	249	5 (F$_1$S−F$_2$S); 12 (F$_1$A−F$_2$A)	62	–	5 (F$_{16}$)
1A	− 99.14			30	0	<3 (F$_{13}$)
2S	− 101.09	249		–	0	5 (F$_8$)
2A	− 104.40			76	15	4 (F$_5$)
9S	− 100.15	251	10 (F$_9$S−F$_{10}$S); 11 (F$_{10}$A−F$_9$A)	33	0	<3 (F$_7$)
9A	− 105.06			66	15	
10S	− 105.16	252		66	17	<3 (F$_{15}$)
10A	− 100.08			32	0	<3 (F$_{12}$)

(b)

Position	δ (ppm)	$^3J_{ortho}$ (Hz)	$^4J_{meta}$ (Hz)	$^5J_{para}$ (Hz)	$^7J_{pseudo-gem}$ (Hz)
5	− 126.68	–	6	7	12
7	− 136.94	20	6	–	9
8	− 135.84		–	7	7
12	− 136.33	21	7	10	12
13	− 133.42		7	12	–
15	− 132.00	20	7	10	7
16	− 132.66		7	12	9

Table 6. NMR data for the (a) aliphatic fluorines and (b) aromatic fluorines in compound 5 in benzene-d_6

(a)

Position	δ (ppm)	^2J (Hz)	^3J (Hz)	$^4J_{syn}$ (Hz)	$^5J_{syn}$ (Hz)	Other ^nJ (Hz)
1S	-98.69	252	9 (F_1A–F_2A)	58	–	4 (F_{16})
1A	-99.48			37	<3	5 (F_{13})
2S	-96.98	255		–	<3	4 (F_8)
2A	-101.25			70	11	
9S	-101.52	251	9 (F_9S–$F_{10}S$); 11 ($F_{10}A$–F_9A)	42	5	5 (F_7)
9A	-103.89			61	10	4 (F_5)
10S	-104.73	253		61	12	5 (F_{15})
10A	-101.42			39	0	

(b)

Position	δ (ppm)	$^3J_{ortho}$ (Hz)	$^4J_{meta}$ (Hz)	$^5J_{para}$ (Hz)	$^7J_{pseudo-gem}$ (Hz)
5	-133.84	–	7	8	12
7	-149.73	21	7	–	10
8	-137.58		–	8	8
12	-136.51	18	6	10	12
13	-134.01		7	11	–
15	-132.05	20	7	10	8
16	-133.03		6	11	10

Table 8. NMR data for the (a) aliphatic fluorines and (b) aromatic fluorines in compound 7 in benzene-d_6

(a)

Position	δ (ppm)	^2J (Hz)	^3J (Hz)	$^4J_{syn}$ (Hz)	$^5J_{syn}$ (Hz)	Other ^nJ (Hz)
1S	-98.23	251	9 (F_1S–F_2S)	23	–	<3 (F_{14})
1A	-104.94			70	31	<3 (F_{12})
2S	-105.78	248		–	26	
2A	-97.24			20	0	
9S	-105.89	250	9 (F_9A–$F_{10}A$); 11 (F_9S–$F_{10}S$)	75	11	
9A	-99.00			33	0	3 (F_5)
10S	-99.94	252		35	0	<3 (F_{16})
10A	-105.76			67	11	

(b)

Position	δ (ppm)	$^3J_{ortho}$ (Hz)	$^4J_{meta}$ (Hz)	$^5J_{para}$ (Hz)	$^7J_{pseudo-gem}$ (Hz)
5	-127.77	–	4	10	8
7	-138.00	22	4	–	10
8	-128.42		–	10	10
12	-133.00	20	4	6	8
13	-131.29		4	8	–
15	-135.39	21	4	6	10
16	-135.11		4	8	10

Table 7. NMR data for the (a) aliphatic fluorines and (b) aromatic fluorines in compound 6 in benzene-d_6

(a)

Position	δ (ppm)	^2J (Hz)	^3J (Hz)	$^4J_{syn}$ (Hz)	$^5J_{syn}$ (Hz)	Other ^nJ (Hz)
1S	-98.55	252	5 (F_1S–F_2A); 9 (F_1S–F_2S)	22	–	5 (F_{15})
1A	-105.20			70	32	4 (F_{12})
2S	-105.00	250		–	31	3 (F_7)
2A	-97.75			20	0	
9S	-105.76	250	8 (F_9A–$F_{10}A$); 9 (F_9S–$F_{10}S$)	74	10	
9A	-99.45			38	4	4 (F_5)
10S	-100.27	251		37	0	3 (F_{16})
10A	-105.65			63	10	3 (F_{13})

(b)

Position	δ (ppm)	$^3J_{ortho}$ (Hz)	$^4J_{meta}$ (Hz)	$^5J_{para}$ (Hz)	$^7J_{pseudo-gem}$ (Hz)
5	-128.75	–	5	8	10
7	-140.13	23	5	–	10
8	-128.89		–	8	10
12	-133.10	24	4	8	10
13	-131.51		7	6	–
15	-135.23	21	7	8	10
16	-134.91		4	6	10

Table 9. NMR data for the (a) aliphatic fluorines and (b) aromatic fluorines in compound 8 in benzene-d_6

(a)

Position	δ (ppm)	^2J (Hz)	^3J (Hz)	$^4J_{syn}$ (Hz)	$^5J_{syn}$ (Hz)	Other ^nJ (Hz)
1S	-98.69	252	4 (F_1S–F_2A); 8 (F_1S–F_2S)	22	–	4 (F_{15})
1A	-105.21			69	36	4 (F_{12})
2S	-102.98	251		–	37	5 (F_7)
2A	-97.84			20	5	
9S	-105.21	251	10 (F_9A–$F_{10}A$); 10 (F_9S–$F_{10}S$)	73	10	3 (F_7); 4 (F_8)
9A	-99.61			43	5	5 (F_5)
10S	-100.92	251		41	5	5 (F_{16})
10A	-105.40			59	10	2 (F_{13})

(b)

Position	δ (ppm)	$^3J_{ortho}$ (Hz)	$^4J_{meta}$ (Hz)	$^5J_{para}$ (Hz)	$^7J_{pseudo-gem}$ (Hz)
5	-129.24	–	6	10	10
7	-144.26	22	6	–	10
8	-130.60		–	10	10
12	-133.54	20	0	10	10
13	-131.92		5	10	–
15	-135.14	20	5	10	10
16	-134.80		0	10	10

wileyonlinelibrary.com/journal/mrc
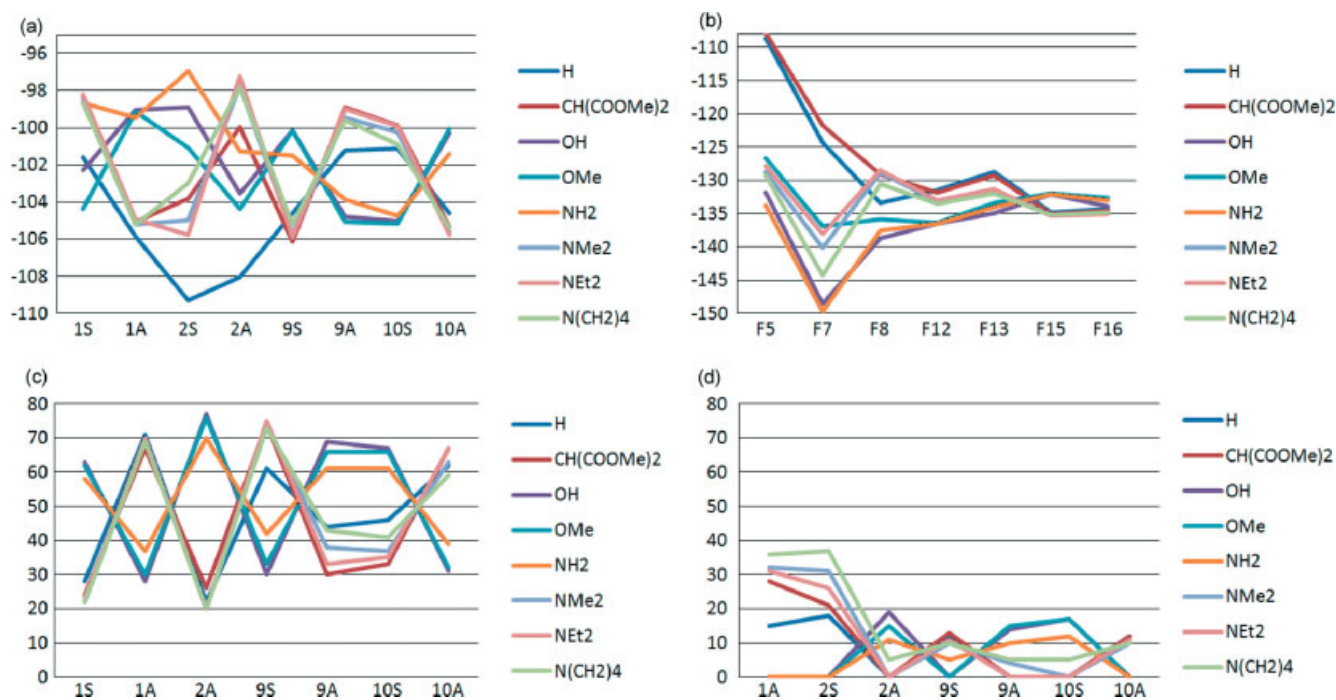
Figure 5. Trends in the chemical shifts of the aliphatic (a) and aromatic (b) fluorines and in $^4J_{syn}$ (c) and $^5J_{syn}$ (d).

This agrees well with the $^{19}F-^1H$ HOESY spectrum of 7 in toluene-d_8 at $-60\,^{\circ}C$, where the two ethyl groups are non-equivalent. Two methylene protons, at 3.55 and 3.26 ppm, of the same methylene group (they both coupled with the methyl protons at 1.23 ppm) displayed scalar coupling (anti-phase peaks) with F_5 at -127.4 ppm. The methyl protons at 1.23 ppm displayed coupling with F_{13} at -129.8 ppm. The barriers to rotation ($\Delta G^{\#}$ 298) in compounds 6 and 7 are 10.9 and 12.3 kcal/mol, respectively.

Analysis of calculated coupling constants, $^4J(F_5,F_9S)$, $^5J(F_5,F_{10}S)$ and $^4J(F_{12},F_{10}S)$ and $^5J(F_{12},F_9S)$ in compound 4

Calculated spin–spin coupling constants include the four isotropic Ramsey[16] terms, FC, spin-dipolar (SD), PSO and diamagnetic spin orbit (DSO) contributions calculated at the HF/6-311+G(d,p)//B3LYP/EPR-III level. The coupling pathway involved in both $^4J_{syn}$ can transmit through-space both the PSO and FC terms; the latter is positive and its magnitude depends strongly on the F–F distance, the former is negative and its magnitude depends rather markedly, besides other effects, on the strain along the coupling pathway.[15] The latter depends on the overlapping of both fluorine electronic clouds.

A comparison between the calculated and the experimental $^4J_{syn}$ in compounds 1, 4 and 7 is given in Tables 10–12, respectively. The calculated values compare well with the experimental ones and mimic the dependence of the coupling constants on the F–F distances. Data shown in Tables 10–12 indicate that the major contribution to $^4J_{syn}$ comes from the FC term. The F_m–F_n distances reported in Tables 10–12 are shorter than twice the fluorine van der Waals radius (2×1.47 Å). This suggests that this FC term is mainly transmitted through-space due to the fluorine lone pairs overlap. These results are in good agreement with similar data discussed, among other authors, by Arnold *et al.*[17] Data displayed in Tables 10–12 suggest that the SD term is also transmitted through-space and that it depends more strongly on the F–F distance than the FC term.

The transmission mechanisms of the $^5J_{syn}$ couplings cannot be rationalized on the same grounds as those operating for $^4J_{syn}$. In order to disentangle this conundrum, calculated and experimental four $^5J_{syn}$ couplings for compounds 1, 4 and 7 are collected in Tables 13–15, respectively, where the largest $^5J_{syn}$ couplings are also dominated by the FC term like $^4J_{syn}$ couplings shown in Tables 10–12. Besides, the calculated values reproduce well the experimental ones in particular $^5J_{syn}(F_9S-F_{12}) \approx 0$ and $^5J_{syn}(F_{10}A-F_7) \approx 0$ in compound 4, and $^5J_{syn}(F_9A-F_{16}) \approx 0$ and $^5J_{syn}(F_{10}S-F_5) \approx 0$ in compound 7. It is obvious that transmission mechanisms of the FC term for $^4J_{syn}$ are notably different than those for the FC term of $^5J_{syn}(F_mF_n)$ since for all four couplings given in Tables 13–15, the distances between the coupling nuclei are always larger than twice the van der Waals radius and, therefore, any direct $^5J_{syn}(FC)$ through-space coupling should be ruled out.

In order to rationalize the behavior of $^5J_{syn}(F_mF_n)$ (FC) couplings in compounds 1–8, it must be recalled that it is now known that the FC interaction is transmitted through each molecular electronic system in the same manner as the Fermi hole[18,19] is. This observation led, during the last few years, to understand several unusual pathways for transmitting the FC term.[20–22] Since many years ago, it is known that the FC term can be transmitted by an intermediate moiety,[23,24] like for instance, that suggested by Mallory *et al.*,[25] in which a coupling $^6J_{F-F} = 6.4$ Hz is transmitted through a phenyl ring. A recently reported unusual case is that of the stereo-chemical dependence of the $^2J_{CH}$ coupling involving the formyl proton in several 5-X-furfurals[26] where an FC pathway involving the overlap between the lone-pairs of both oxygen atoms is activated for the *syn* but not for the *anti* conformations.

Keeping these ideas in mind and scrutinizing carefully data collected in Tables 11 and 14, it is chosen to study the pairs of couplings $^4J(F_5,F_9S)$, $^5J(F_5,F_{10}S)$ and $^4J(F_{12},F_{10}S)$ and $^5J(F_{12},F_9S)$ in compound 4 as model systems to get physical insight into the experimental trends depicted in Tables 10–15. The following working hypothesis is advanced: the intermediate moiety for

Table 10.	Comparison between total calculated and experimental values (Hz) of four relevant $^4J_{syn}(F_mF_n)$ in compound 1[a,b]						
F_m	F_n	J^{FC}	J^{SD}	J^{PSO}	J^{DSO}	J_{total}	J_{exp}	$d(F_n - F_m)$ (Å)
$F_{10}A$	F_{16}	79.02	3.24	− 1.25	2.01	83.03	62	2.54
F_9S	F_5	78.55	3.11	− 1.39	1.92	82.08	61	2.54
F_9A	F_7	32.72	0.99	− 9.26	1.78	26.24	44	2.69
$F_{10}S$	F_{12}	32.85	1.04	− 8.49	1.77	27.18	46	2.69

Table 11.	Comparison between total calculated and experimental values of four relevant $^4J_{syn}(F_mF_n)$ in compound 4[a,b]						
F_m	F_n	J^{FC}	J^{SD}	J^{PSO}	J^{DSO}	J_{total}	J_{exp}	$d(F_n - F_m)$
$F_{10}A$	F_{16}	26.35	0.75	− 8.83	1.77	20.04	32	2.71
F_9S	F_5	27.16	0.86	− 9.27	1.82	20.57	33	2.70
F_9A	F_7	79.03	3.53	− 8.42	2.04	76.18	66	2.54
$F_{10}S$	F_{12}	79.21	3.56	− 7.93	2.05	76.89	66	2.54

[a] All values are in Hz.
[b] Distances are in Å.

Table 12.	Comparison between total calculated and experimental values of four relevant $^4J_{syn}(F_mF_n)$ in compound 7[a,b]						
F_m	F_n	J^{FC}	J^{SD}	J^{PSO}	J^{DSO}	J_{total}	J_{exp}	$d(F_n - F_m)$
$F_{10}A$	F_{16}	77.23	3.83	− 8.64	2.04	74.46	67	2.54
F_9S	F_5	77.43	3.87	− 8.02	2.04	75.32	75	2.52
F_9A	F_7	27.12	0.81	− 8.99	1.84	20.78	33	2.70
$F_{10}S$	F_{12}	28.21	0.85	− 9.43	1.91	21.54	35	2.68

[a] All values are in Hz.
[b] Distances are in Å.

Table 13.	Comparison between total calculated and experimental values of four relevant $^5J_{syn}(F_mF_n)$ in compound 1[a,b]						
F_m	F_n	J^{FC}	J^{SD}	J^{PSO}	J^{DSO}	J_{total}	J_{exp}	$d(F_n-F_m)$
F_9A	F_{16}	0.18	0.93	− 0.62	0.07	0.56	0	4.31
$F_{10}S$	F_5	0.11	0.94	− 0.42	0.02	0.65	0	4.31
F_9S	F_{12}	9.75	2.03	− 2.31	1.54	11.02	12	3.13
$F_{10}A$	F_7	9.45	2.09	− 2.16	1.56	10.94	12	3.13

[a] All values are in Hz.
[b] Distances are in Å.

Table 14.	Comparison between total calculated and experimental values of four relevant $^5J_{syn}(F_mF_n)$ in compound 4[a]						
F_m	F_n	J^{FC}	J^{SD}	J^{PSO}	J^{DSO}	J_{total}	J_{exp}	$d(F_n-F_m)$
F_9A	F_{16}	14.99	2.1	− 3.8	1.77	15.06	15	2.99
$F_{10}S$	F_5	15.06	2.21	− 3.83	1.79	15.23	17	2.99
F_9S	F_{12}	0.22	0.85	− 0.66	0.01	0.42	0	4.37
$F_{10}A$	F_7	0.20	0.86	− 0.63	0.01	0.44	0	4.36

[a] All values are in Hz.
[b] Distances are in Å.

Table 15.	Comparison between total calculated and experimental values of four relevant $^5J_{syn}(F_mF_n)$ in compound 7[a]						
F_m	F_n	J^{FC}	J^{SD}	J^{PSO}	J^{DSO}	J_{total}	J_{exp}	$d(F_n - F_m)$
F_9A	F_{16}	0.21	0.75	− 0.55	0.01	0.42	0	4.29
$F_{10}S$	F_5	0.22	0.76	− 0.52	0.01	0.47	0	4.29
F_9S	F_{12}	16.12	2.11	− 3.87	1.79	16.15	11	3.08
$F_{10}A$	F_7	16.27	2.34	− 3.91	1.81	16.51	11	3.05

[a] All values are in Hz.
[b] Distances are in Å.

transmitting $^5J_{syn}(F_mF_n)$ in compound 4 is just a fluorine atom. For instance, for $^5J_{syn}(F_9A-F_{16})$ coupling, the role of the intermediate F atom is played by $F_{10}A$. Such coupling pathway might operate like this; the overlap between the $F_{10}A$ and F_{16} lone-pairs yields $^4J_{syn}(F_{10}A-F_{16})$ (FC) = 26 Hz, which is by far transmitted through-space due to the overlap of their electronic clouds and 'contaminates' the $F_{10}A$ lone-pairs with the F_{16} FC spin information. Besides, it should be transmitted to F_9A in much the same way as the FC term of *vicinal* $^3J_{syn}(F_{10}A-F_9A)$ is.[27] The following observation is compatible with this hypothesis, the corresponding $^3J_{anti}(F_{10}A-F_9S)$ and $^5J_{syn}(F_9S-F_{16})$ couplings were not observed.

Since the optimized $F_{10}A-F_9A$ distance is only 2.42 Å, the FC term of $^3J_{syn}(F_{10}A-F_9A)$ would be in part transmitted through-space from $F_{10}A$ to F_9A, yielding $^5J_{syn}(F_9A-F_{16})$ (FC) = 15 Hz, determining a 'second leg' for the coupling pathway for the latter. Of course, the same rationalization holds considering the reverse coupling pathway, i.e. $F_9A-F_{10}A-F_{16}$ instead of $F_{16}-F_{10}A-F_9A$ since always $^nJ_{ab} = {}^nJ_{ba}$.

This hypothesis seems to work well when the corresponding $^4J_{syn}$ is approximately within the 15–30 Hz range. For larger $^4J_{syn}(F_mF_n)$ (Tables 10–12) values, this hypothesis seems to fail since the corresponding $^5J_{syn}(F_mF_n)$ (Tables 13–15) is close to 0 Hz. Theoretical considerations must provide an answer to this last observation. An intuitive and easy to apply qualitative approach to detect possible FC coupling pathways in a given compound was recently reported. Such an approach was dubbed FCCP-CMOs, FC coupling pathways studied by analyzing CMOs.[28] Only a brief and minimal description of that approach is given here. Adequate details can be found in the quoted bibliography and in references cited therein. In the next subsection, such approach is applied to compare FC pathways for $^5J_{syn}(F_{10}S-F_5)$ with $^5J_{syn}(F_9S-F_{12})$, and for $^4J_{syn}(F_9S-F_5)$ with $^4J_{syn}(F_{10}S-F_{12})$ coupling constants in compound 4.

FCCP-CMOs approach applied to get insight into $^5J_{syn}(F_{10}S-F_5)$(FC), $^5J_{syn}(F_9S-F_{12})$(FC), $^4J_{syn}(F_9S-F_5)$(FC) and $^4J_{syn}(F_{10}S-F_{12})$(FC) coupling constants in 4

Brief notions on the qualitative FCCP-CMOs method necessary to understand the discussion presented in this subsection is given here. It is recalled that CMOs satisfy the Pauli Exclusion Principle and, therefore, the Fermi hole spans the whole spatial region of each CMO. Since it is known that the FC term is transmitted like the Fermi hole,[18,19] the spin information corresponding to the FC term also spans that spatial region. Therefore, the studied coupling constants $^nJ^{FC}_{F,F'}$, are expressed in terms of CMOs; where n stands for the number of formal bonds separating the coupling fluorine nuclei (Eqn 1). To identify relevant CMOs for a given coupling, its expression in terms of the polarization propagator approach, PP, at the random phase approximation (RPA), Eqn (2) is employed

$$^nJ^{FC}_{F,F'} = \sum_{ia,jb} {}^nJ^{FC}_{ia,jb}(F, F') \quad (1)$$

where i and j stand for occupied CMOs, whereas a and b stand for vacant CMOs, and each sum term in Eqn (1) can be written as in Eqn (2),[29]

$$^nJ^{FC}_{ia,jb}(F, F') = {}^3W_{ia,jb}[U^{FC}_{ia,F}U^{FC}_{jb,F'} + U^{FC}_{ia,F'}U^{FC}_{jb,F}] \quad (2)$$

where $(U_{ia,F}(U_{jb,F})$ are the so-called 'perturbators', i.e. the matrix elements $U^{FC}_{ia,x} = \langle i | \delta(\vec{r_X}) | a \rangle$ of the FC operator, $\delta(\vec{r_X})$, i.e. the Dirac's

delta function, between the occupied i (j) and vacant a (b) CMOs evaluated at the sites of the F (F') coupling nuclei,

$$^3W_{ia,jb} = ({}^3A - {}^3B)^{-1}_{ia,jb} \quad (3)$$

are the elements of the triplet PP matrix, and they can be expressed in terms of orbital energies, ε, and molecular orbital integrals, Eqn (4)

$$^3A_{ia,jb} = (\varepsilon_a - \varepsilon_i)\delta_{ab}\delta_{ij} - \langle aj|bi \rangle \quad \text{and} \quad {}^3B_{ia,jb} = \langle ab|ji \rangle \quad (4)$$

Each sum term in Eqn (1), $^nJ^{FC}_{ia,jb}(XY)$, is dubbed an FCCP and depends on both the $^3W_{ia,jb}$ matrix element and on the 'perturbators', $U_{ia,F}(U_{jb,F})$, i.e. a given FCCP is non-negligible whenever both types of terms are simultaneously significant. Therefore, here is described very briefly under which conditions those types of terms are significant.

The $^3W_{ia,jb}$ diagonal matrix elements, i.e. those satisfying $i = j$ and $a = b$, are larger[29a] than non-diagonal terms. They depend explicitly and strongly on the energy gap between the vacant a and the occupied i CMO; $\Delta_{a,i} = \varepsilon_a - \varepsilon_i$ and decrease when increasing $\Delta_{a,i}$, and vice versa. However, it is important to point out that, for a given coupling constant, many diagonal elements of the PP matrix are also negligible small.

'Perturbator' $U_{ia,F}$ terms are important whenever there is a substantial overlap between $i = j$ and $a = b$ orbitals at the positions of both coupling nuclei. For a significant diagonal PP matrix element one occupied and one vacant CMO determine an efficient FCCP; those orbitals can be spotted observing their respective NBO expansions. In fact, for being an efficient FCCP, the occupied CMO should be contributed by σ-bonds or lone-pairs (excluding those of pure π character) containing the coupling nuclei, and the unoccupied CMO should be contributed by anti-bonding σ-orbitals containing the coupling nuclei. It is also recalled that only the diagonal $^3W_{ia,jb}$ matrix elements depend explicitly and strongly on the virtual-occupied orbital energy gap, $\Delta_{a,i}\varepsilon = (\varepsilon_a - \varepsilon_i)$. With these ideas in mind, it is easy to identify the CMOs that could constitute efficient FCCPs for a given coupling constant.

Applying the practical rules described above possible analogous FCCPs are compared for $^5J_{syn}(F_{10}S-F_5)$ with $^5J_{syn}(F_9S-F_{12})$ in compound 4. When comparing coupling pathways for $^4J_{syn}(F_9S-F_5)$ and $^4J_{syn}(F_{10}S-F_{12})$, some caution should be taken since they are by far dominated by the coupling pathway determined by the coupling nuclei lone-pair overlapping. Physically, in this coupling pathway the FC term is transmitted by exchange interactions taking place between the coupling nuclei overlapping electronic clouds and, therefore, it is expected that only occupied CMOs should determine the main coupling pathways for the FC terms of $^4J_{syn}(F_9S-F_5)$ and $^4J_{syn}(F_{10}S-F_{12})$ couplings.

In the Supporting Information, CMO (occupied and vacant) whose NBOs expansions contain any pair of the following four atoms, F_5, F_9S, $F_{10}S$ and F_{12}, except those occupied CMOs with an energy lower than -0.679055 a.u. or higher than $+1$ a.u. are displayed since they would involve a very large $\Delta_{a,i} = (\varepsilon_a - \varepsilon_i)$ energy gap and therefore their contributions to coupling constants relevant to this qualitative analysis should be too small to yield insight into the main factors determining the observed experimental trends. CMO expansions in terms of NBOs as given by the Weinhold *et al.*'s 5.0 NBO program[5] are considered; they are displayed using conventions used in the outputs of that program. Briefly, they are (i) CMOs are numbered
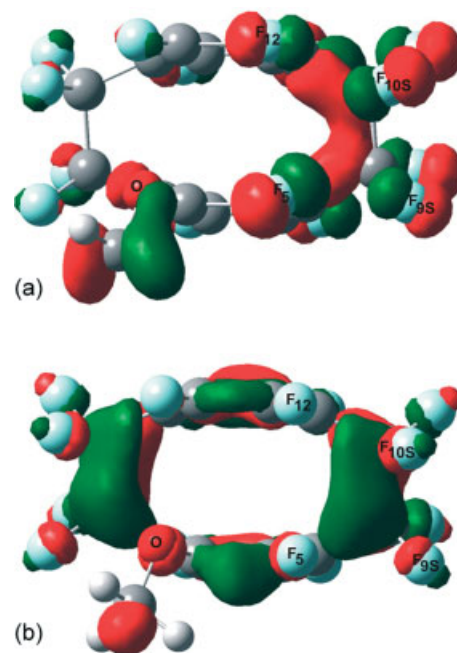
Table 16. Expansion of relevant CMOs in terms of NBOs in compound 4

Occupied CMOs	Vacant CMOs
CMO 109 (occ): $\varepsilon = -0.419280$ a.u.; 0.370* [103]: LP (2) F_5(lp); -0.283* [114]: LP (2) F_9S(lp); 0.240* [121]: LP (3) F_{10}S(lp)	CMO 129 (vir): $\varepsilon = 0.024166$ a.u.; -0.277* [437]: BD* (1) $C_{12}-F_{12}$*; -0.256* [471]: BD* (1) C_5-F_5*
CMO 108 (occ): $\varepsilon = -0.424528$ a.u.; -0.247* [94]: LP (2) F_{12}(lp); 0.234* [103]: LP (2) F_5(lp); 0.233* [121]: LP (3) F_{10}S(lp)	CMO 130 (vir): $\varepsilon = 0.039066$ a.u.; -0.257* [451]: BD* (1) $C_{10}-F_{10}$S*; 0.242* [471]: BD* (1) C_5-F_5*
CMO 106 (occ): $\varepsilon = -0.430080$ a.u.; -0.268* [114]: LP (2) F_9S(lp); -0.230* [103]: LP (2) F_5(lp)	MO 131 (vir): $\varepsilon = 0.050564$ a.u.; -0.300* [437]: BD* (1) $C_{12}-F_{12}$*; 0.244* [471]: BD* (1) C_5-F_5*
CMO 103 (occ): $\varepsilon = -0.440928$ a.u.; -0.381* [94]: LP (2) F_{12}(lp); 0.273* [120]: LP (2) F_{10}S(lp); -0.268* [121]: LP (3) F_{10}S(lp)	MO 136 (vir): $\varepsilon = 0.099446$ a.u.; -0.235* [471]: BD* (1) C_5-F_5*; 0.225* [437]: BD* (1) $C_{12}-F_{12}$*
CMO 100 (occ): $\varepsilon = -0.456086$ a.u.; -0.373* [103]: LP (2) F_5(lp); -0.366* [114]: LP (2) F_{10}S(lp); -0.325* [94]: LP (2) F_{12}(lp)	MO 140 (vir): $\varepsilon = 0.141878$ a.u.; 0.365* [471]: BD* (1) C_5-F_5*; 0.257* [437]: BD* (1) $C_{12}-F_{12}$*
CMO 98 (occ): $\varepsilon = -0.471647$ a.u.; -0.326* [103]: LP (2) F_5(lp); 0.253* [121]: LP (3) F_{10}S(lp); 0.249* [94]: LP (2) F_{12}(lp); 0.225* [115]: LP (3) F_9S(lp)	

Only NBOs involving F_5, F_9S, F_{10}S and F_{12} are displayed. The complete expansions of these relevant CMOs in terms of NBOs are given in the Supporting Information.

Figure 6. Visualization of CMO transmission mechanisms for $^4J_{syn}(F_9S-F_5)$ and $^4J_{syn}(F_{10}S-F_{12})$ and $^5J_{syn}(F_{10}S-F_5)$ couplings in compound 4. (a) Occupied CMO 98 and (b) vacand CMO 130.

from lower to higher energy, indicating if they are occupied of vacant CMOs; CMO energies are given in atomic units, (ii) the first number, followed by an asterisk, when squared corresponds to each NBO contribution with a threshold of 5%; (iii) the second number, in square brackets, corresponds to the NBO numbering, (iv) next, the NBO type is shown followed by the atom or atoms involved in it (numbered as in the Gaussian 03 program output), i.e. core, lone-pair; bonding, antibonding, or Rydberg orbitals, respectively.

In Table 16, the abridged Supporting Information displaying for each CMO only the relevant NBOs whose atoms participate explicitly in $^5J_{syn}(F_{10}S-F_5)$, $^5J_{syn}(F_9S-F_{12})$, $^4J_{syn}(F_9S-F_5)$, and $^4J_{syn}(F_{10}S-F_{12})$ coupling constants is shown. Occupied CMOs are presented from highest to lowest orbital energies, whereas vacant CMOs are presented from lowest to highest energies to visualize easily the corresponding energy gaps. There are only five CMO(vir) containing NBOs that include more than one of the atoms involved in coupling constants mentioned above. It is observed that four of them include the F_5 and F_{12} atoms, but neither F_{10}S nor F_9S atoms. These correspond to the transmission of the *pseudo-gem* $^9J(F_{12}-F_5)$ but not to the $^5J_{syn}(F_9S-F_{12})$ coupling. Therefore, the only virtual CMO that could be significant for transmitting any of the $^5J_{syn}(F_{10}S-F_5)$, $^5J_{syn}(F_9S-F_{12})$, $^4J_{syn}(F_9S-F_5)$ and $^4J_{syn}(F_{10}S-F_{12})$ couplings is the CMO(vir) 130. The respective virtual transitions should be the following three, (I) CMO(occ)109 → CMO(vir)130, (II) CMO(occ)108 → CMO(vir)130 and (III) CMO(occ)98 → CMO(vir)130.

Obviously, the virtual transition (I) corresponds to the coupling pathway mentioned in the working hypothesis: CMO(occ)109 contains these lone-pair orbitals: $LP_2(F_5)$, $LP_3(F_{10}S)$ and $LP_2(F_9S)$ where the F_9S plays the role of the 'intermediate F atom' for transmitting the FC term of $^5J_{syn}(F_{10}S-F_5)$ coupling. It is highlighted that the CMO(vir)130 does not include the $\sigma^*(C_9-F_9S)$ anti-bonding orbital since $^4J_{syn}(F_9S-F_5)$ coupling is transmitted by the overlap of LP(2) of F_9S and LP(2) of F_5. Virtual transition (II) contributes also to the $^5J_{syn}(F_{10}S-F_5)$ coupling transmission but its energy gap is about 0.005 a.u. larger than in (I). The same can be said about the virtual transition (III); in this case, the respective energy gap is about 0.062 a.u. larger than in (I), showing a notably smaller efficiency for transmitting the $^5J_{syn}(F_{10}S-F_5)$ coupling.

There are not equivalent virtual transitions to transmit the FC term of $^5J_{syn}(F_9S-F_{12})$ since there is no virtual CMO containing the equivalent to CMO(vir)130, i.e. a CMO(vir) containing the NBOs $\sigma^*(C_9-F_9S)$ and $\sigma^*(C_{12}-F_{12})$. Thus, the 'towards' conformation of the upper deck for compound 4 leads to an important distortion of the $F_{12}-C_{12}-C_{11}-C_{10}-F_{10}S$ moiety, which inhibits the existence of a virtual CMO containing simultaneously those two NBO anti-bonding orbitals, rendering a very inefficient coupling pathway for $^5J_{syn}(F_9S-F_{12})$. This distortion renders also a much shorter $F_{12}-F_{10}S$ distance, increasing notably the overlap between their electronic clouds, increasing the through-space transmission of $^4J_{syn}(F_{10}S-F_{12})$. Such distortion is also observed in Table 12 comparing the F_9A-F_{16} distance, 2.99 Å, with that of F_9S-F_{12}, i.e. 4.37 Å. Such distortions should originate mainly in the $\sigma_{C_{10}-F_{10}S}$ bond (and, of course, in its anti-bonding orbital) when the geometry of this compound adopts a 'towards'' geometry. All three CMOs(occ)108, 103 and 98 contribute to the through-space via overlapping the lone pairs $^4J_{syn}(F_{10}S-F_{12})$ coupling. It is highlighted that these transmissions are not affected by the respective CMO orbital energies since they are transmitted by exchange interactions taking place in the lone-pair overlap region.

Similarly, $^4J_{syn}(F_9S-F_5)$ is transmitted by CMOs(occ) 109, 106, 100 and 98, i.e. such couplings do not require of anti-bonding orbitals for the transmission of their FC terms.

A pictorial representation of trends described in the last paragraph is obtained by plotting the corresponding CMO orbitals. Two of them, one occupied, CMO 98, and one virtual, CMO 130, are plotted in Fig. 6. The former shows the overlap between the aromatic F_5 and F_{12} $LP_2(F)$ non-bonding electron pairs and the aliphatic $F_{10}S$ and F_9S $LP(3)$ non-bonding electron pairs. They transmit the FC term of $^4J_{syn}(F_{10}S-F_{12})$ and $^4J_{syn}(F_9S-F_5)$ without requiring a virtual CMO orbital. On the other hand, the virtual CMO 130 is efficient for contributing to the FC transmission of the $^5J_{syn}(F_{10}S-F_5)$ coupling since it involves both the $\sigma^*(C_5-F_5)$ and $\sigma^*(C_{10}-F_{10})$ anti-bonding orbitals. On the other hand, CMO 130 is not efficient for transmitting the $^5J_{syn}(F_9S-F_{12})$ since, although it contains the $\sigma^*(C_{12}-F_{12})$, anti-bonding orbital, contribution from the $\sigma^*(C_9-F_9S)$ is negligible as compared with that of the $\sigma^*(C_{10}-F_{10})$ anti-bonding orbital.

Concluding Remarks

The results presented in this work show the important structural information that can be obtained performing a detailed analysis of long-range J_{FF} coupling constants in perfluoroparacyclophanes. In particular, compound 4 is taken as a model compound to study, from a theoretical point of view, the influence of a skewed geometry on the $^4J(F_9S,F_5)$, $^4J(F_{10}S,F_{12})$, $^5J(F_{10}S,F_5)$ and $^5J(F_9S,F_{12})$ couplings displayed in Tables 10–15. To this end, the FCCP-CMO approach was applied to rationalize the unusual trends observed for the FC term of such couplings, i.e. the respective FC contributions are, $^4J(F_9S,F_5) = 27$ Hz, $^4J(F_{10}S,F_{12}) = 79$ Hz; $^5J(F_{10}S,F_5) = 15$ Hz and $^5J(F_9S,F_{12}) = 0$ Hz. This quite unusual behavior for the FC term is rationalized as follows, where the atom numbering shown in Fig. 1 is employed. That pair of couplings, $^5J_{syn}(F_{10}S-F_5)$ and $^4J_{syn}(F_9S-F_5)$, are observed when F_9S is not too close to F_5 and the FC term of $^5J_{syn}(F_{10}S-F_5)$ is transmitted mainly via the intermediate F_9S atom. On the other hand, for the pair of couplings $^5J_{syn}(F_9S-F_{12})$ and $^4J_{syn}(F_{10}S-F_{12})$, $F_{10}S$ and F_{12} atoms are notably closer to each other than F_9S and F_5 in $^4J(F_9S,F_5)$. As a consequence, the FC term of $^4J_{syn}(F_{10}S-F_{12})$ is notably larger than in the former case and the corresponding bonds $\sigma(C_{10}-F_{10}S)$ and $\sigma(C_{12}-F_{12})$ are almost contained in the same plane. The F_{12} spin information associated with the FC term cannot be transmitted to F_9S because the distortion of the $\sigma(C_{10}-F_{10}S)$ bonding orbital leads to an anti-bonding $\sigma(C_{10}-F_{10}S)$ orbital that cannot enter into a virtual CMO containing simultaneously the $\sigma(C_{12}-F_{12})$ anti-bonding orbital. In this manner, the FC term of $^5J(F_9S,F_{12})$ is inhibited, in agreement with the experimental observations.

It is highlighted that both $^4J_{syn}(F_9S-F_5)$ and $^4J_{syn}(F_{10}S-F_{12})$ are by far transmitted through-space by the overlap of the corresponding LP(F) lone pairs and, therefore, they do not require the presence of virtual CMOs to be transmitted. This contrasts with the FC term of $^5J_{syn}(F_{10}S-F_5)$, where the 'second leg' of its coupling pathway, i.e. from F9S to F10S, requires for its transmission at least one virtual CMO containing simultaneously both $\sigma(C_{10}-F_{10}S)$ and $\sigma(C_5-F_5)$ anti-bonding orbitals.

In Tables 11, 12, 14 and 15 is shown that for compounds 4 and 7, which show as preferential 'towards' and 'away' conformations, respectively, the roles played by $^5J_{syn}(F_{10}S-F_5)$ and $^5J_{syn}(F_9S-F_{12})$ are exchanged. The same holds for $^4J_{syn}(F_9S-F_5)$ and $^4J_{syn}(F_{10}S-F_{12})$ couplings. Therefore, these five-bond $^5J_{syn}(F-F)$

and four-bond $^4J_{syn}(F-F)$ couplings are useful 'probes' to identify the 'away' and 'towards' conformation for the upper deck in the type of perfluorocyclophanes studied in this work.

For compound 1, (R = H) it is found that the preferential conformation is 'away' indicating that the R size is not the only interaction determining the conformation of the type of monosubstituted perfluoroparacyclophanes studied in this work. Apparently, an important role determining such conformation is played by an attractive interaction between the aromatic systems of both the benzene rings.

Supporting information

Supporting information may be found in the online version of this article.

References

[1] L. H. Zhang, K. Ogawa, I. Ghiviriga, W. R. Dolbier, *J. Org. Chem.* **2009**, *74*, 6831.
[2] I. Ghiviriga, F. Dulong, W. R. Dolbier, *Magn. Reson. Chem.* **2009**, *47*, 313.
[3] gMNR website: http://home.cc.umanitoba.ca/~budzelaa/gNMR/gNMR.html [15 September 2010].
[4] M. J. Frisch, G. W. Trucks, H. B. Schlegel, G. E. Scuseria, M. A. Robb, J. R. Cheeseman, J. A. Montgomery Jr, T. Vreven, K. N. Kudin, J. C. Burant, J. M. Millam, S. S. Iyengar, J. Tomasi, V. Barone, B. Mennucci, M. Cossi, G. Scalmani, N. Rega, G. A. Petersson, H. Nakatsuji, M. Hada, M. Ehara, K. Toyota, R. Fukuda, J. Hasegawa, M. Ishida, T. Nakajima, Y. Honda, O. Kitao, H. Nakai, M. Klene, X. Li, J. E. Knox, H. P. Hratchian, J. B. Cross, V. Bakken, C. Adamo, J. Jaramillo, R. Gomperts, R. E. Stratmann, O. Yazyev, A. J. Austin, R. Cammi, C. Pomelli, J. W. Ochterski, P. Y. Ayala, K. Morokuma, G. A. Voth, P. Salvador, J. J. Dannenberg, V. G. Zakrzewski, S. Dapprich, A. D. Daniels, M. C. Strain, O. Farkas, D. K. Malick, A. D. Rabuck, K. Raghavachari, J. B. Foresman, J. V. Ortiz, Q. Cui, A. G. Baboul, S. Clifford, J. Cioslowski, B. B. Stefanov, G. Liu, A. Liashenko, P. Piskorz, I. Komaromi, R. L. Martin, D. J. Fox, T. Keith, M. A. Al-Laham, C. Y. Peng, A. Nanayakkara, M. Challacombe, P. M. W. Gill, B. Johnson, W. Chen, M. W. Wong, C. Gonzalez, J. A. Pople, *Revision E.01*, Gaussian: Wallingford, CT, **2004**.
[5] E. D. Glendening, J. K. Badenhoop, A. E. Reed, J. E. Carpenter, J. A. Bohmann, C. M. Morales, F. Weinhold, *NBO 5.0*, Theoretical Chemistry Institute: University of Wisconsin, Madison, **2001**.
[6] M. G. Hogben, W. A. G. Graham, *J. Am. Chem. Soc.* **1969**, *91*, 283.
[7] L. Ernst, K. Ibrom, *Magn. Reson. Chem.* **1997**, *35*, 868.
[8] I. D. Rae, D. A. Burgess, S. Bombaci, M. L. Baron, M. L. Woolcock, *Aust. J. Chem.* **1984**, *37*, 1437.
[9] B. W. Gung, J. C. Amicangelo, *J. Org. Chem.* **2006**, *71*, 9261.
[10] J. P. Gallivan, D. A. Dougherty, *Org. Lett.* **1999**, *1*, 103.
[11] Y.-X. Lu, J.-W. Wang, Q.-S. Yu, *Int. J. Quantum Chem.* **2007**, *107*, 1479.
[12] M. Barfield, B. Chakrabarti, *Chem. Rev.* **1969**, *69*, 757.
[13] T. Schaefer, R. Schwenk, C. J. Macdonald, W. F. Reynolds, *Can. J. Chem.* **1968**, *46*, 2187.
[14] F. B. Mallory, C. W. Mallory, K. E. Butler, M. B. Lewis, A. Q. Xia, E. D. Luzik, L. E. Fredenburgh, M. M. Ramanjulu, Q. N. Van, M. M. Francl, D. A. Freed, C. C. Wray, C. Hann, M. Nerz-Stormes, P. J. Carroll, L. E. Chirlian, *J. Am. Chem. Soc.* **2000**, *122*, 4108.

Magnetic
Resonance in
Chemistry

[15] J. E. Peralta, V. Barone, R. H. Contreras, D. G. Zaccari, J. P. Snyder, *J. Am. Chem. Soc.* **2001**, *123*, 9162.

[16] N. F. Ramsey, *Phys. Rev.* **1953**, *91*, 303.

[17] W. D. Arnold, J. H. Mao, H. H. Sun, E. Oldfield, *J. Am. Chem. Soc.* **2000**, *122*, 12164.

[18] A. Soncini, P. Lazzeretti, *J. Chem. Phys.* **2003**, *119*, 1343.

[19] N. Castillo, C. F. Matta, R. J. Boyd, *J. Chem. Inf. Model* **2005**, *45*, 354.

[20] R. H. Contreras, A. L. Esteban, E. Díez, N. J. Head, E. W. Della, *Mol. Phys.* **2006**, *104*, 485.

[21] F. P. dos Santos, C. F. Tormena, R. H. Contreras, R. Rittner, A. Magalhaes, *Magn. Reson. Chem.* **2008**, *46*, 107.

[22] G. F. Gauze, E. A. Basso, R. H. Contreras, C. F. Tormena, *J. Phys. Chem. A* **2009**, *113*, 2647.

[23] M. A. Natiello, R. H. Contreras, *Chem. Phys. Lett.* **1984**, *104*, 568.

[24] R. H. Contreras, J. E. Peralta, *Prog. Nucl. Mag. Res. Sp.* **2000**, *37*, 321.

[25] F. B. Mallory, C. W. Mallory, M. B. Baker, *J. Am. Chem. Soc.* **1990**, *112*, 2577.

[26] C. Perez, R. Suardiaz, P. J. Ortiz, R. Crespo-Otero, G. M. Bonetto, J. A. Gavin, J. M. García de la Vega, J. S. Fabian, R. H. Contreras, *Magn. Reson. Chem.* **2008**, *46*, 846.

[27] P. F. Provasi, S. P. A. Sauer, *J. Chem. Theory Comput.* **2006**, *2*, 1019.

[28] R. H. Contreras, G. Gotelli, L. C. Ducati, T. M. Barbosa, C. F. Tormena, *J. Phys. Chem. A* **2010**, *114*, 1044.

[29] (a) J. Oddershede, in *Advances in Quantum Chemistry*, vol. 11 (Ed.: P.-O. Löwdin), Academic Press: London, **1978**, p. 275; (b) A. C. Diz, C. G. Giribet, M. C. Ruiz de Azúa, R. H. Contreras, *Int. J. Quantum Chem.* **1990**, *37*, 663; (c) R. H. Contreras, M. C. Ruiz de Azúa, C. G. Giribet, G. A. Aucar, R. Lobayan de Bonczok, *J. Mol. Struct. Theochem.* **1993**, *284*, 249.